NANO EXPRESS   **Open Access**

Graphene-supported SnO$_2$ nanoparticles prepared by a solvothermal approach for an enhanced electrochemical performance in lithium-ion batteries

Bei Wang[1], Dawei Su[1], Jinsoo Park[2], Hyojun Ahn[2] and Guoxiu Wang[1,2*]

Abstract

SnO$_2$ nanoparticles were dispersed on graphene nanosheets through a solvothermal approach using ethylene glycol as the solvent. The uniform distribution of SnO$_2$ nanoparticles on graphene nanosheets has been confirmed by scanning electron microscopy and transmission electron microscopy. The particle size of SnO$_2$ was determined to be around 5 nm. The as-synthesized SnO$_2$/graphene nanocomposite exhibited an enhanced electrochemical performance in lithium-ion batteries, compared with bare graphene nanosheets and bare SnO$_2$ nanoparticles. The SnO$_2$/graphene nanocomposite electrode delivered a reversible lithium storage capacity of 830 mAh g^{-1} and a stable cyclability up to 100 cycles. The excellent electrochemical properties of this graphene-supported nanocomposite could be attributed to the insertion of nanoparticles between graphene nanolayers and the optimized nanoparticles distribution on graphene nanosheets.

Keywords: SnO$_2$, Graphene nanosheets, Nanocomposite, Lithium-ion batteries

Background

Graphene has been emerged as a rising star in materials science and as an excellent candidate for many applications due to its unique two dimensional (2D) nanostructure [1], outstanding electrical properties [2], and ultrahigh specific surface area [3]. The applications of graphene include gas molecule adsorption [4], quantum dots [5], transistors [6], lithium-ion batteries [7], supercapacitors [8], lithium air batteries [9], and drug delivery [10]. In particular, graphene has attracted worldwide attention for energy storage and conversion. With the formation of sandwich-like three dimensional (3D) nanostructured composite materials, the restacking of graphene nanosheets (GNS) can be effectively prevented and therefore the electrochemical properties of the nanocomposite electrodes could be significantly improved by using nanocrystallines to insert between layers of graphene nanosheets [3,11].

SnO$_2$ has been examined as an anode material for lithium-ion batteries with a high theoretical capacity of 782 mAh g^{-1} [12]. SnO$_2$ forms metal alloys when reacting with lithium, leading to reversible transformations between lithium tin alloys (Li$_x$Sn) and tin metal when the lithiation and delithiation proceed. However, the capacity of bulk SnO$_2$ electrode fades quickly during prolonged cycling [13]. To further improve the electrochemical performance and the cycle life of SnO$_2$ electrodes for long-term cycling, one approach is to synthesize nanosized SnO$_2$ crystals with different morphologies, such as nanowires [14], nanotubes [15], and mesoporous structure [16]. These nanostructured SnO$_2$ materials were reported to deliver greatly enhanced specific capacities with durable cycling stabilities. In order to mechanically buffer the volume expansion associated with the charge/discharge processes in the lithium-ion cells, the formation of SnO$_2$/graphene nanocomposites has also been proved to be feasible. Many methods have been implemented to distribute SnO$_2$ nanocrystals on graphene nanosheets, including *in situ* chemical preparation [13,17], reassembling process [18], gas–liquid interfacial synthesis [19], as well as hydrothermal and solvothermal methods [20,21].

* Correspondence: Guoxiu.Wang@uts.edu.au
[1]Centre for Clean Energy Technology, School of Chemistry and Forensic Science, University of Technology, City Campus, Broadway, Sydney, NSW 2007, Australia
[2]School of Materials Science and Engineering, Gyeongsang National University, 900 Gazwa-dong, Jinju, Gyeongnam 660-701, South Korea

In this paper, we employ a facile solvothermal technique to disperse SnO_2 nanoparticles with a controlled size on graphene nanosheets. The as-prepared SnO_2/GNS nanocomposite showed uniform SnO_2 nanoparticles distribution and significantly improved electrochemical properties, compared with bare graphene nanosheets and SnO_2 nanoparticles. The solvothermal approach developed in this investigation could be used for the synthesis of other metal oxide/graphene nanocomposites.

Methods

Graphene oxide (GO) powders were prepared via a chemical approach derived from Hummers' method [22], according to the previously reported procedure [7]. In a typical synthesis process, 40 mg GO was firstly dispersed in 40 ml ethylene glycol by ultrasonification for 1 h, followed by the addition of 0.1 mmol $SnCl_2 \cdot 2H_2O$ powders. The mixture was vigorously stirred for half an hour, and then transferred to a 50 ml Teflon lined autoclave, which was sealed and maintained in an oven at 160°C for 6 h. Afterwards, the black precipitates (SnO_2/GNS) were collected, washed with deionized water and ethanol to remove the impurities, and isolated by vacuum filtration. The product was then dried in a vacuum oven at 60°C, and further sintered at 300°C for 4 h in argon to increase the crystallinity. For the comparison, bare SnO_2 nanoparticles were also synthesized by the same experimental procedure without the presence of GO in the mixture solution.
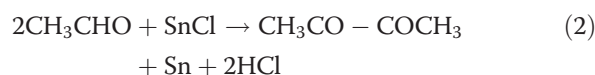
The X-ray diffraction (XRD) pattern of the as-synthesized material was measured using a Siemens D5000 X-ray diffractometer (Siemens Company, Wittelsbacherplatz 2, Munich, Germany) from 10° to 80° under a scan rate of 1° min^{-1}. The Raman measurement of the SnO_2/GNS nanocomposite was conducted on a confocal Micro Raman Spectrometer with LabRAM HR system (HORIBA Korea Ltd., Pucheon, Kyunggido Korea) using a 632.8 nm He-Ne laser source. The spectra were recorded in the range of 200 to 2,000 cm^{-1} with accumulated scans for an enhanced resolution. Field emission scanning electron microscope (FESEM) observations were performed using a Zeiss Supra 55VP FESEM with an Oxford energy dispersive spectrometry system (Carl Zeiss Nanotechnology Center, Oberkochen, Germany). The transmission electron microscopy (TEM) analysis was carried out using a Jeol 2011 TEM facility (JEOL Ltd., Tokyo, Japan). The graphene (carbon) content in the composite material was determined by thermogravimetric analysis (TGA) on a TGA/DTA analyzer (TA Instruments, SDT 2960 module, New Castle, DE, USA) in air at 10°C min^{-1} ranging from room temperature to 1,000°C.

CR2032 coin cells were assembled in an argon-filled glove box (Unilab, M Braun Inertgas-Systeme GmbH, Garching, Germany) in which the levels of moisture and oxygen were controlled to be less than 0.1 ppm. The electrodes were made by mixing 80 wt% SnO_2/GNS active materials, 10 wt% carbon black, and 10 wt% polyvinylidene fluoride binder in the *N*-methyl-2-pyrrolidone solvent to form a slurry. Then, the slurry was coated on copper foil substrate. Lithium foils were used as the negative electrodes. The electrolyte was 1 M $LiPF_6$ in ethylene carbonate and dimethyl carbonate (1:1). Cyclic voltammetry (CV) tests were carried out on an electrochemistry workstation (CHI660D, CH Instrument, Inc., Austin, TX, USA) at a scan rate of 0.1 mV s^{-1} vs. Li/Li$^+$ reference electrode in the voltage range of 0.01 to 3 V. Galvanostatic charge/discharge measurements were conducted on the Neware battery tester (Neware Co.,Ltd., Shenzhen, China) with a current rate of 0.1 C for 100 cycles. Electrochemical impedance spectroscopy was performed on the same electrochemistry workstation. The frequency was set in 0.01 Hz–100 kHz with the amplitude of 5 mV. The charge/discharge performance was also investigated for bare graphene nanosheets and SnO_2 nanoparticles as a comparison.

Results and discussion

Figure 1 shows a schematic diagram of the formation of the SnO_2/GNS nanocomposite. Firstly, Sn^{2+} ions were attracted to GO nanosheets in the ethylene glycol (EG) solution. Then, the anchored Sn^{2+} ions were reduced by EG via the following two-step reactions:

$$2HOCH_2 - CH_2OH \rightarrow 2CH_3CHO + 2H_2O \qquad (1)$$

$$2CH_3CHO + SnCl \rightarrow CH_3CO - COCH_3 \\ + Sn + 2HCl \qquad (2)$$

Simultaneously, GO nanosheets were also gradually reduced by EG to form graphene nanosheets. As EG is a mild reducing agent, the reduction processes take a long time (6 h) to complete at the high temperature (160°C). Then, the formed Sn nanoparticles were further oxidized by oxygen to become SnO_2 nanoparticles during the cooling period. Consequently, the SnO_2/GNS nanocomposite was obtained under the assistance of EG which acted not only as a dispersing agent but also as a reducing agent.

XRD patterns of the SnO_2/GNS nanocomposite and graphene were shown in Figure 2. In Figure 2a, X-ray diffraction lines of well-crystallized SnO_2 were indexed to the tetragonal rutile SnO_2 phase, which is consistent with the Joint Committee on Powder Diffraction
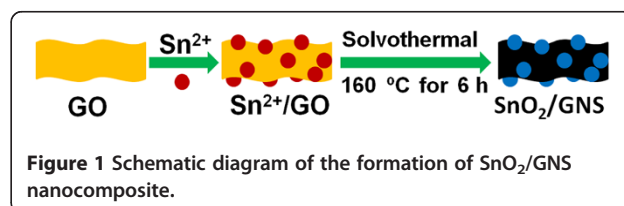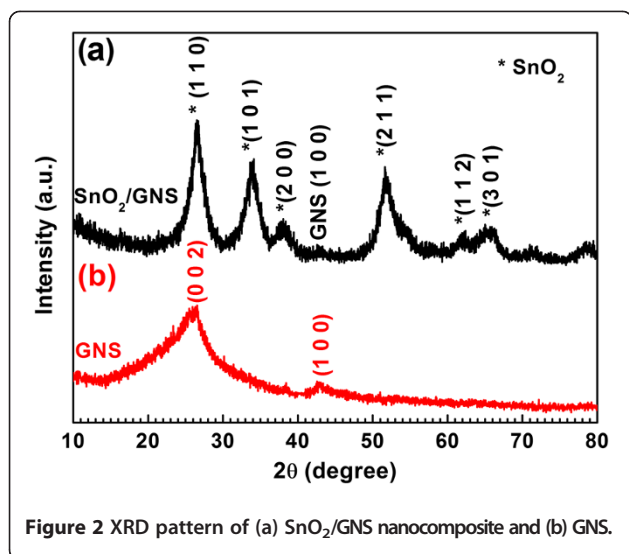

Figure 1 Schematic diagram of the formation of SnO_2/GNS nanocomposite.

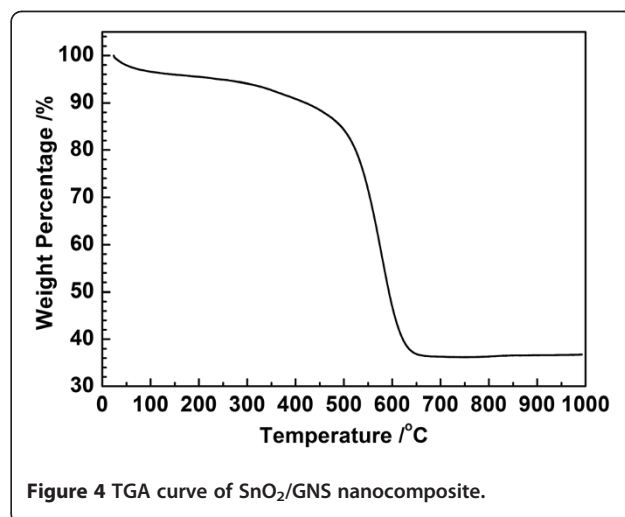**Figure 2** XRD pattern of (a) SnO_2/GNS nanocomposite and (b) GNS.

Standards card 01–0657. The weak peak of graphene is also visible at 42° in the composite, which matches the diffraction peak (1 0 0) marked on the XRD pattern of bare graphene nanosheets (as shown in Figure 2b). XRD confirmed the coexisting phases of rutile SnO_2 and graphene and the formation of SnO_2/GNS nanocomposite.
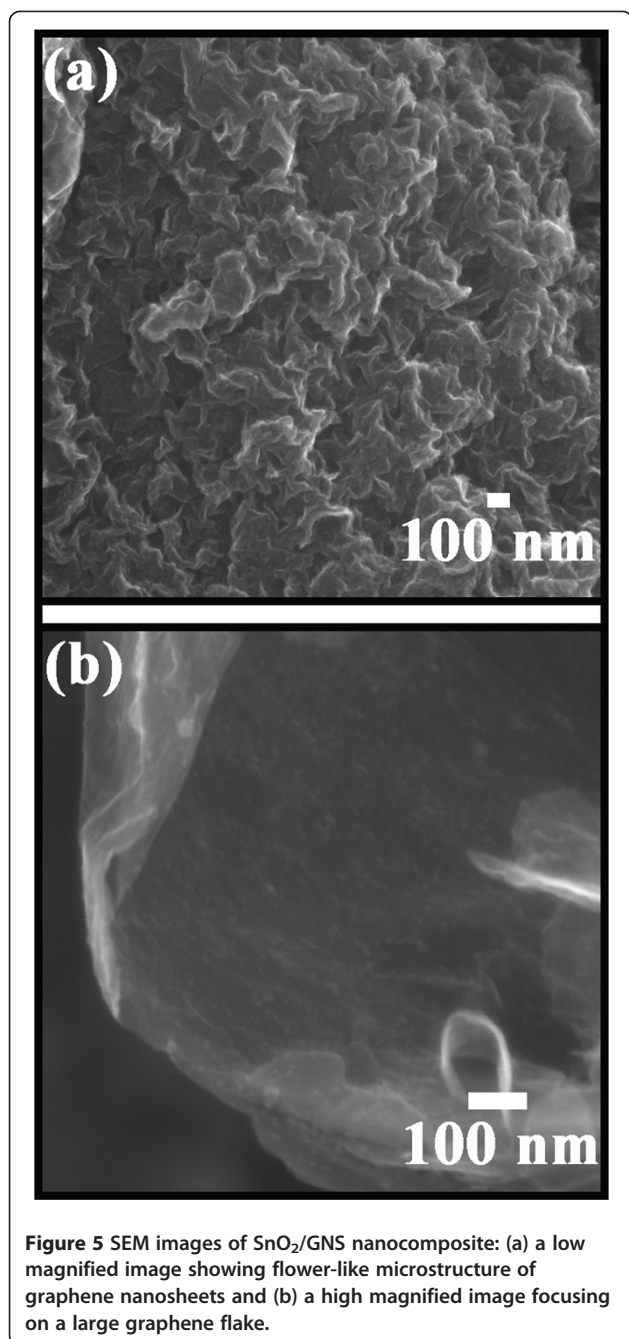
Raman spectra of the as-prepared SnO_2/GNS nanocomposite and bare GNS are shown in Figure 3. It can be seen that both of them show high-intensity D band and G band at around 1,327 and 1,587 cm^{-1}, respectively. The D band is stronger than the G band, and the D/G intensity ratio increased significantly compared to pristine graphite [23], which confirmed the existence of graphene nanosheets in the composite material. The D/G
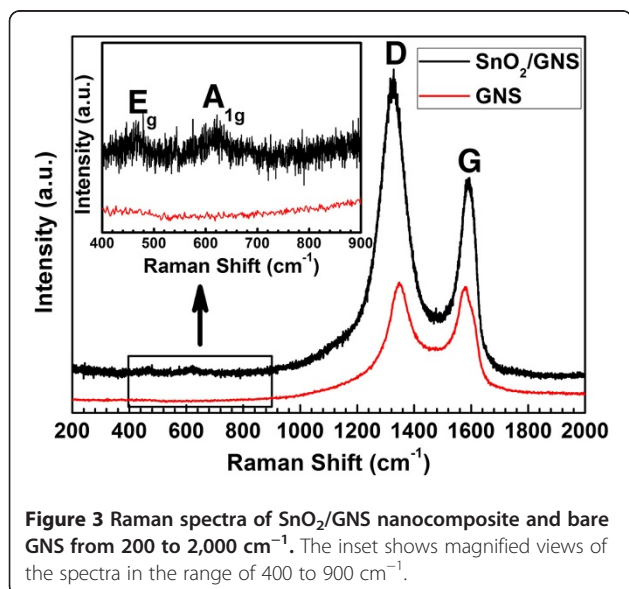
intensity ratio of the SnO_2/GNS nanocomposite is higher than that of the bare GNS, indicating the decrease of the sp^2 carbon domains when SnO_2 nanoparticles were inserted between graphene nanosheets [24]. The inset in Figure 3 displayed magnified Raman spectra in the range of 400 to 900 cm^{-1} of both SnO_2/GNS and bare GNS. Two weak peaks were found at 465 and 620 cm^{-1} in the Raman spectrum of the SnO_2/GNS nanocomposite, which can be assigned to the E_g and A_{1g} active modes of SnO_2 crystallines [25]. For the bare GNS, no Raman peak in this range was observed. TGA was employed to determine the weight composition of the SnO_2/GNS nanocomposite (as shown in Figure 4). The dramatic weight loss from 500°C to 630°C is associated with the burning of graphene in air. SnO_2 in the nanocomposite was stable up to 1,000°C. Therefore, the composition of the SnO_2/GNS nanocomposite was calculated to be 36.3 wt% SnO_2 and 63.7 wt% graphene.

Figure 5 displays FESEM images of the SnO_2/GNS nanocomposite. Corrugated graphene nanosheets are well expanded and form flower-like nanostructure (Figure 5a). A magnified scanning electron microscope (SEM) view further revealed details of a large, flat graphene nanosheet (Figure 5b). Tiny SnO_2 nanoparticles were found anchored on this graphene flake. Figure 6 shows a TEM image of the SnO_2/GNS nanocomposite. A large amount of SnO_2 nanoparticles were homogeneously distributed on the graphene nanosheets as shown in Figure 6a. The inset shows the selected area electron diffraction pattern (SAED). The diffraction rings were indexed as the crystal planes (1 1 0), (1 0 1), (2 0 0), (2 1 1), (2 1 0) of SnO_2, which clearly confirms the presence of SnO_2 in the nanocomposite material. High resolution TEM (HRTEM) was performed on a few SnO_2 nanoparticles (Figure 6b). SnO_2 nanocrystals were densely packed on the surface of graphene nanosheets. Two crystal planes were indexed to be
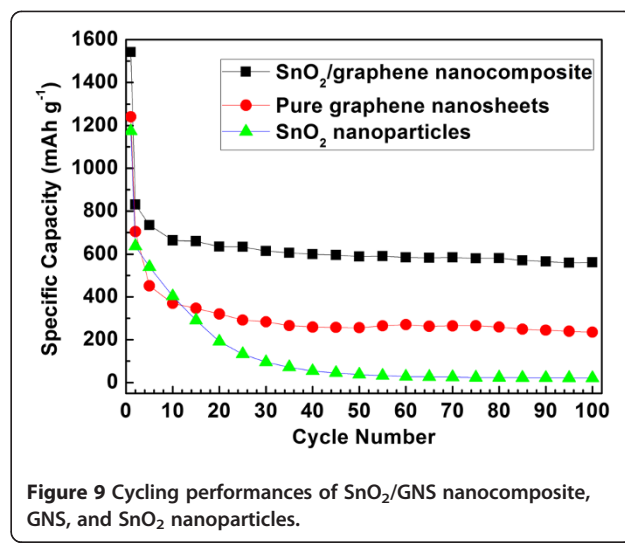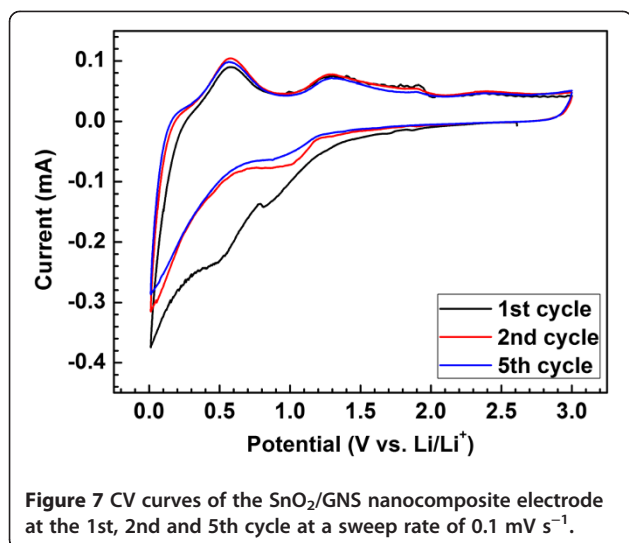

Figure 3 Raman spectra of SnO_2/GNS nanocomposite and bare GNS from 200 to 2,000 cm^{-1}. The inset shows magnified views of the spectra in the range of 400 to 900 cm^{-1}.

Figure 4 TGA curve of SnO_2/GNS nanocomposite.

Figure 5 SEM images of SnO₂/GNS nanocomposite: (a) a low magnified image showing flower-like microstructure of graphene nanosheets and (b) a high magnified image focusing on a large graphene flake.

Figure 6 TEM images of SnO₂/GNS nanocomposite: *top* image shows a low magnified image exhibiting homogenous distribution of SnO₂ nanoparticles on graphene nanosheets. The inset shows the corresponding SAED ring pattern, where crystal planes (1 1 0), (1 0 1), (2 0 0), (2 1 1), (2 1 0) of SnO₂ are indexed; *bottom* image shows an HRTEM image focusing on a few SnO₂ nanoparticles with indexed (1 0 0) and (1 1 0) crystal planes.

(1 0 0) and (1 1 0) of SnO_2. The particle size of SnO_2 was determined to be around 5 nm.

Figure 7 presents typical CV characteristics related to the lithiation and delithiation processes of the SnO_2/GNS nanocomposite in the lithium-ion cell. A small cathodic peak appears at 0.8 V in the first cycle which can be attributed to the formation of the solid electrolyte interphase layer. Another small reduction peak located around 0.06 V could be due to the reactions between lithium and SnO_2 nanoparticles to form Li_xSn alloys, while the insertion of lithium in graphene nanosheets could be identified
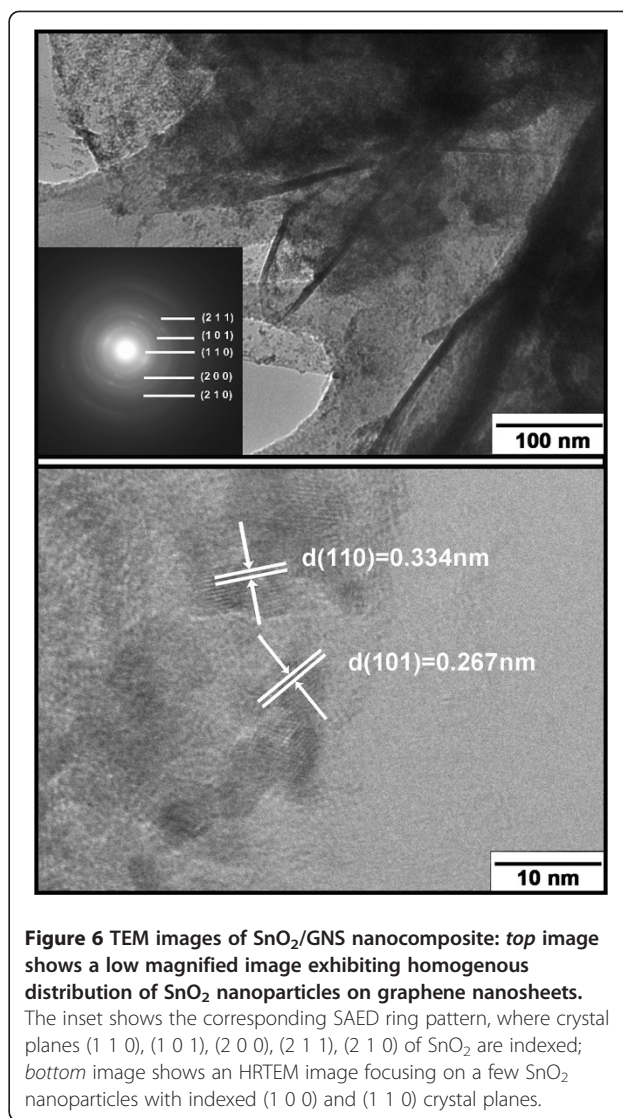
as the reduction peak at 0.01 V. There are three oxidation peaks located around 0.13, 0.55, and 1.3 V, respectively. They correspond to different oxidation reactions during the charge process. The first anodic peak at 0.13 V represents the lithium extraction from graphene nanosheet. The 0.55 V oxidation peak can be assigned to the dealloying of Li_xSn, showing a reversible process. The third weak oxidation at 1.3 V could be resulted from the partial transformation of Sn metal to SnO_2 [26,27]. The high reversibility of the CV curves further confirmed the reversible redox reactions occurring in the lithium-ion cell between lithium and SnO_2/GNS nanocomposite.
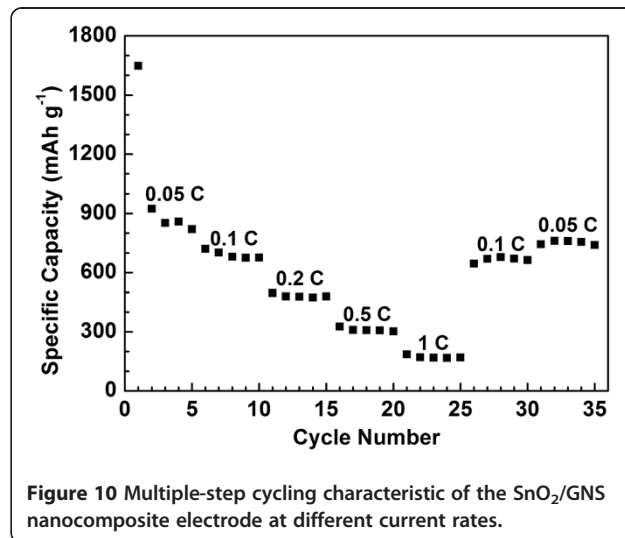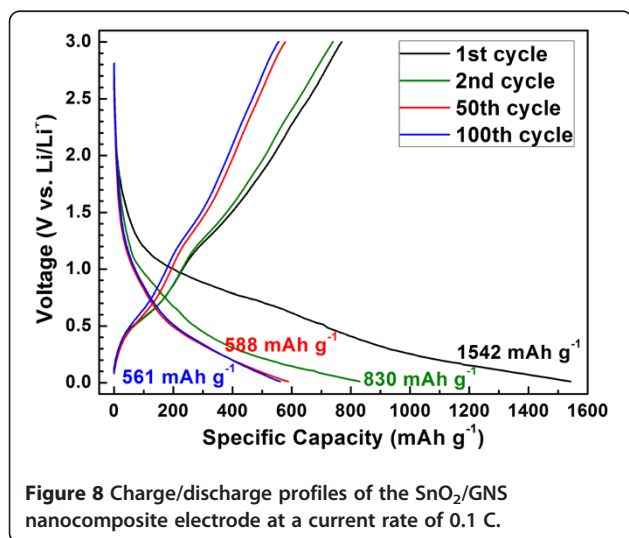
Figure 8 shows the charge/discharge profiles of the SnO_2/GNS nanocomposite electrode in different cycles at a current rate of 0.1 C. It can be seen that the SnO_2/GNS electrode delivered a discharge capacity of 1,542 mAh g⁻¹ in the first cycle. From the second cycle, the nanocomposite electrode exhibited highly reversible charge and
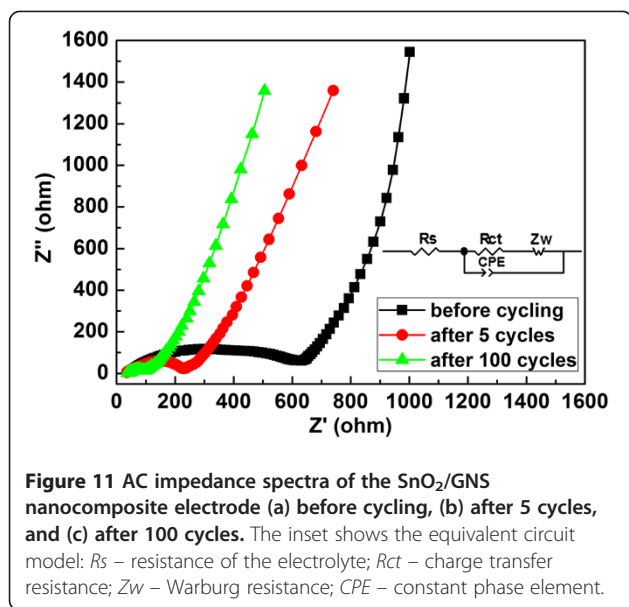
Figure 7 CV curves of the SnO_2/GNS nanocomposite electrode at the 1st, 2nd and 5th cycle at a sweep rate of 0.1 mV s^{-1}.

Figure 9 Cycling performances of SnO_2/GNS nanocomposite, GNS, and SnO_2 nanoparticles.

discharge capacities. The maximum reversible discharge capacity of 830 mAh g^{-1} was achieved in the second discharge cycle. Specific discharge capacities of 588 and 561 mAh g^{-1} were obtained in the 50th and 100th cycle respectively, which indicates a very stable cycling performance. Significant improvement on the specific capacities has been achieved. Figure 9 shows the long-term cycling properties of the SnO_2/GNS nanocomposite, bare graphene nanosheets and SnO_2 nanoparticles at a 0.1 C current rate. The SnO_2/GNS nanocomposite electrode demonstrated the highest reversible capacities and the best cycling stability. The nanocomposite electrode delivered a discharge capacity of 1,542 mAh g^{-1} in the first cycle and maintained stable capacities from the second cycle for 100 cycles with an excellent capacity retention. On the other hand, the bare GNS electrode showed a large irreversible capacity with lower reversible discharge capacities in 100 cycles. The capacities of SnO_2 nanoparticles decrease quickly upon cycling.

The retained capacity was less than 30 mAh g^{-1} in the 100th cycle. Figure 10 demonstrates multiple-step cycling characteristics of the SnO_2/GNS nanocomposite electrode at 0.05 to 0.1, 0.2, 0.5, and 1 C and then reversing back to 0.1 and 0.05 C. The nanocomposite electrode was capable to deliver stable specific capacities at various current rates and recover substantial capacities without obvious capacity decline when returning to lower current rates. This indicated a fully reserved microstructure of the nanocomposite electrode after cycling at higher current rates.

Figure 11 shows the alternating current (AC) impedance spectra of the SnO_2/GNS nanocomposite electrode before cycling, after 5 cycles and after 100 cycles and the equivalent circuit model (inset). The intercept on the Z' axis at the high frequency region represents the resistance of the electrolyte (R_s), which is 56.2 Ω for a fresh cell. The electrolyte resistance slightly decreased to 35 Ω after 5 cycles and remained nearly unchanged after 100 cycles (36.2 Ω).

Figure 8 Charge/discharge profiles of the SnO_2/GNS nanocomposite electrode at a current rate of 0.1 C.

Figure 10 Multiple-step cycling characteristic of the SnO_2/GNS nanocomposite electrode at different current rates.

Figure 11 AC impedance spectra of the SnO$_2$/GNS nanocomposite electrode (a) before cycling, (b) after 5 cycles, and (c) after 100 cycles. The inset shows the equivalent circuit model: *Rs* – resistance of the electrolyte; *Rct* – charge transfer resistance; *Zw* – Warburg resistance; *CPE* – constant phase element.

The diameters of the semicircles on the spectra implied the charger transfer resistances (R_{ct}) at the electrolyte/electrode interface. It should be noted that the initial charge transfer resistance was 575.9 Ω then gradually decreased to 242.5 Ω (after 5 cycles) and 95.25 Ω (after 100 cycles) upon prolonged cycling. The significantly decreased charge transfer resistance could benefit for an enhanced cycle life of the SnO$_2$/GNS nanocomposite electrode. The overall electrochemical performance of the SnO$_2$/GNS nanocomposite was improved as graphene nanosheets supported SnO$_2$ nanoparticles on their layered nanostructure. The inserted SnO$_2$ nanoparticles reduce the stacking degree of graphene nanosheets and also contribute to the reversible lithium storage. Graphene nanosheets in the nanocomposite not only accommodate the volume change associated with the reactions between lithium and SnO$_2$ nanoparticles, but also provide electrical conductance for the electrodes. For the SnO$_2$/GNS nanocomposite prepared by the solvothermal method, the electrochemical properties were further improved due to the optimized nanoparticle distribution and small particle size of SnO$_2$. The well-dispersed SnO$_2$ nanoparticles effectively prevent the formation of agglomerates on graphene nanosheets, which induces an enhanced electrochemical performance.

Conclusions

A facile solvothermal preparation method has been developed to synthesize the SnO$_2$/GNS nanocomposite with a uniform nanoparticle distribution. The as-prepared SnO$_2$/GNS nanocomposite exhibited an improved lithium storage capacity and cycling performance compared to bare GNS and bare SnO$_2$ nanoparticles. The presence of GNS in the nanocomposite could increase the electrical conductivity and buffer the volume expansion associated with the lithiation and delithiation processes, leading to a significantly enhanced electrochemical performance. The solvothermal approach might be applicable for rapid and effective synthesis of other metal oxide/graphene nanocomposites.

Abbreviations
GNS, Graphene nanosheets; GO, Graphene oxide.

Competing interests
The authors declare that they have no competing interests.

Authors' contributions
BW designed and carried out the experimental work, conducted basic characterizations of the sample, undertook all the electrochemical tests, analyzed all the data, and wrote the manuscript. DS performed the TEM observations. JP obtained the Raman spectra of the samples. AH and GW supervised the research work and GW critically revised the manuscript. All authors read and approved the final manuscript.

References
1. Geim AK, Noveselov KS: **The rise of graphene.** *Nature Mater* 2007, **6**:183–191.
2. Castro Neto AH, Guinea F, Peres NMR, Novoselov KS, Geim AK: **The electronic properties of graphene.** *Rev Mod Phys* 2009, **81**:109–162.
3. Stankovich S, Dikin DA, Dommett GHB, Kohlhaas KM, Zimney EJ, Stach EA, Piner R, Nguyen ST, Ruoff RS: **Graphene-based composite materials.** *Nature* 2006, **442**:282–286.
4. Schedin F, Geim AK, Morozov SV, Hill EW, Blake P, Katsnelson MI, Novoselov KS: **Detection of individual gas molecules adsorbed on graphene.** *Nature Mater* 2007, **6**:652–655.
5. Ponomarenko LA, Schedin F, Katsnelson MI, Yang R, Hill EW, Novoselov KS, Geim AK: **Chaotic dirac billiard in graphene quantum dots.** *Science* 2008, **320**:356–358.
6. Schwierz F: **Graphene transistors.** *Nature Nanotech* 2010, **5**:487–496.
7. Wang GX, Shen XP, Yao J, Park J: **Graphene nanosheets for enhanced lithium storage in lithium ion batteries.** *Carbon* 2009, **47**:2049–2053.
8. Stoller MD, Park S, Zhu Y, An J, Ruoff RS: **Graphene-based ultracapacitors.** *Nano Lett* 2008, **8**:3498–3502.
9. Sun B, Wang B, Su D, Xiao L, Ahn H, Wang GX: **Graphene nanosheets as cathode catalysts for lithium-air batteries.** *Carbon* 2012, **50**:727–733.
10. Sun XM, Liu Z, Welsher K, Robinson JT, Goodwin A, Zaric S, Dai HJ: **Nano-graphene oxide for cellular imaging and drug delivery.** *Nano Res* 2008, **1**:203–212.
11. Xu C, Wang X, Zhu JW: **Graphene-metal particle nanocomposites.** *J Phys Chem C* 2008, **112**:19841–19845.
12. Idota Y, Kubota T, Matsufuji A, Maekawa Y, Miyasaka T: **Tin-based amorphous oxide: a high-capacity lithium-ion-storage material.** *Science* 1997, **276**:1395–1397.
13. Yao J, Shen XP, Wang B, Liu HK, Wang GX: *In situ* **chemical synthesis of SnO$_2$–graphene nanocomposite as anode materials for lithium-ion batteries.** *Electrochem Commun* 2009, **11**:1849–1852.
14. Park MS, Wang GX, Kang YM, Wexler D, Dou SX, Liu HK: **Preparation and electrochemical properties of SnO$_2$ nanowires for application in lithium-ion batteries.** *Angew Chem Int Ed* 2007, **46**:750–753.
15. Wang Y, Lee JY, Zeng HC: **Polycrystalline SnO$_2$ nanotubes prepared via infiltration casting of nanocystallites and their electrochemical application.** *Chem Mater* 2005, **17**:3899–3903.
16. Wang F, Yao G, Xu MW, Zhao MS, Sun ZB, Song XP: **Large-scale synthesis of macroporous SnO$_2$ with/without carbon and their application as anode materials for lithium-ion batteries.** *J Alloys Compd* 2011, **509**:5969–5973.

17. Li YM, Lv XJ, Lu J, Li JH: **Preparation of SnO$_2$-nanocrystal/graphene-nanosheets composites and their lithium storage ability.** *J Phys Chem C* 2010, **114**:21770–21774.
18. Paek SM, Yoo E, Honma I: **Enhanced cyclic performance and lithium storage capacity of SnO$_2$/graphene nanoporous electrodes with three-dimensionally delaminated flexible structure.** *Nano Lett* 2009, **9**:72–75.
19. Lian PC, Zhu XF, Liang SZ, Li Z, Yang WS, Wang HH: **High reversible capacity of SnO$_2$/graphene nanocomposite as an anode material for lithium-ion batteries.** *Electrochim Acta* 2011, **56**:4532–4539.
20. Ding SJ, Luan DY, Boey FYC, Chen JS, Lou XW: **SnO$_2$ nanosheets grown on graphene sheets with enhanced lithium storage properties.** *Chem Comm* 2011, **47**:7155–7157.
21. Huang XD, Zhou XF, Zhou LA, Qian K, Wang YH, Liu ZP, Yu CZ: **A facile one-step solvothermal synthesis of SnO$_2$/graphene nanocomposite and its application as an anode material for lithium-ion batteries.** *Chem Phys Chem* 2011, **12**:278–281.
22. Hummers WS, Offeman RE: **Preparation of graphitic oxide.** *J Am Chem Soc* 1958, **80**:1339–1340.
23. Wang GX, Yang J, Park J, Gou XL, Wang B, Liu H, Yao J: **Facile synthesis and characterization of graphene nanosheets.** *J Phys Chem C* 2008, **112**:8192–8195.
24. Stankovich S, Dikin DA, Piner RD, Kohlhaas KA, Kleinhammes A, Jia Y, Wu Y, Nguyen ST, Ruoff RS: **Synthesis of graphene-based nanosheets via chemical reduction of exfoliated graphite oxide.** *Carbon* 2007, **45**:1558–1565.
25. Sun SH, Meng GW, Zhang GX, Gao T, Geng BY, Zhang LD, Zuo J: **Raman scattering study of rutile SnO$_2$ nanobelts synthesized by thermal evaporation of Sn powders.** *Chem Phys Lett* 2003, **376**:103–107.
26. Poizot P, Laruelle S, Grugeon S, Dupont L, Tarascon J-M: **Nano-sized transition–metal oxides as negative–electrode materials for lithium-ion batteries.** *Nature* 2000, **407**:496–499.
27. Memir-Cakan R, Hu YS, Antonietti M, Maier J, Titirici M-M: **Facile one-pot synthesis of mesoporous SnO$_2$ microspheres via nanoparticles assembly and lithium storage properties.** *Chem Mater* 2008, **20**:1227–1229.